

Unrevealing Charge Carrier Selective Layer in Silicon Heterojunction Solar Cells via Multifunctional Atomic Force Probes

Yusheng Wang, Zhouhui Xia, Haihua Wu, Shaojuan Li, Tao Wang,* and Baoquan Sun*

The current silicon solar cell with a record efficiency is based on heterojunction contacts that offer carrier selectivity as well as surface passivation simultaneously. One remaining challenge with heterocontacts is the balance between carrier extraction and surface passivation. Here, it is demonstrated that the heterojunction of n-type silicon (N–Si) with the conducting polymer poly(3,4-ethylenedioxythiophene):poly(styrene sulfonate) (PEDOT:PSS) removes this trade-off, utilizing the strong depletion of PEDOT:PSS to realize the excellent carrier selectivity. The near-field optical contrast and surface potential distributions of the PEDOT:PSS/N–Si heterojunction via multifunctional atomic force probes are mapped for the first time. Interestingly, a low dielectric value region is observed in N–Si by using scattering-type scanning near-field optical microscopy on the junction cross-section. A special PEDOT:PSS slope is further fabricated to characterize the dielectric value and surface potential in the PEDOT:PSS side. By combining s-SNOM and scanning Kelvin probe microscopy, a special region in PEDOT:PSS is observed with a sharp surface potential drop and low dielectric value. The results suggest the existence of space charge regions both in N–Si and PEDOT:PSS at the interface. These findings contribute the understanding of the physical properties of the silicon heterojunction and promise potential routes to enhance device efficiency.


The record efficiency silicon solar cell is achieved by choosing carrier-selective heterojunction contacts, which provide high degree of carrier selectivity and excellent interface passivation, simultaneously.^[1] For heterojunction devices, the properties and quality of carrier-selective heterojunction contacts play significant role in the device performance.^[2] It is well known that the interface determines the charge separation and transport in heterojunction solar cells. As a result, it is critical to get insight into the interface of heterojunction solar cell with novel

measurement methods, which helps to understand device working mechanism. Measuring junction position, depth, and electrical potential distribution in this heterojunction solar cell is also useful to control the quality of junction formation. In addition, there is a trade-off between requiring thicker layers for better contact selectivity and suppress contact recombination, while requiring thin layers to reduce carrier extraction losses as well as parasitic absorption.

Regarding to n-type silicon (N–Si) and poly(3,4-ethylenedioxythiophene):poly(styrene sulfonate) (PEDOT:PSS) heterojunction, Price et al. had originally pointed out that the velocity of majority charge carrier transfer at PEDOT:PSS/N–Si contact was several orders smaller than that at the N–Si/Au junction.^[3] The lower majority charge carrier transfer rate contributes to the excellent photo-response properties of this heterojunction. After that, numerous reports have been focused on improving device performance through surface passivation,^[4] back field,^[5] contacting,^[6]

and PEDOT:PSS chemical modification.^[7] In these studies, energy alignment of PEDOT:PSS/N–Si hybrid contact has been described as Schottky junction,^[3,8] where PEDOT:PSS acts as the metallic contact because of its high conductivity, or as quasi-p–n junction,^[9–11] where PEDOT:PSS serves as “p-type” layer, providing charge separation due to its high work function and hole-selective nature. The pioneering work by Erickson et al. proposed a model of strong inversion of the N–Si substrate when contacting with PEDOT:PSS.^[9] A solid evidence provided by a fact that a N–Si-based field-effect transistor with PEDOT:PSS as source and drain electrodes to show the p-type layer formation in the N–Si surface. Following that, this model is further solidified by Jackle et al. through carefully investigating the build-in potential and light on/off saturation current of PEDOT:PSS/N–Si heterojunction.^[10] Their results show that carrier transport in this hybrid contact is governed by minority charge carrier diffusion rather than majority thermionic emission over a barrier, which indicates that PEDOT:PSS/N–Si hybrid contact is more similar to a conventional p–n junction. Herein, a strong inversion layer over a wide range of the Si substrate occurs due to electron

Dr. Y. Wang, Dr. Z. Xia, H. Wu, Dr. S. Li, Prof. T. Wang, Prof. B. Sun
 Jiangsu Key Laboratory for Carbon-Based Functional Materials and Devices
 Institute of Functional Nano and Soft Materials (FUNSOM)
 Soochow University
 Suzhou 215123, P. R. China
 E-mail: wangtao2019@suda.edu.cn; bqsun@suda.edu.cn

 The ORCID identification number(s) for the author(s) of this article can be found under <https://doi.org/10.1002/solr.201900312>.

DOI: 10.1002/solr.201900312

transfer from Si to PEDOT:PSS, and it is very likely that charge redistribution would also occur at the PEDOT:PSS layer. However, there is still no method to characterize charge distribution in the PEDOT:PSS layer near the Si surface. Although the bulk Si and n-type Si nanowires have been investigated,^[12] a spatially resolved method to measure the electrically active doping concentration in PEDOT:PSS is required.

Mid-infrared (MIR) scattering-type scanning near-field optical microscope (s-SNOM) is a powerful technique to detect the free carrier response in metallic^[13] and doped-semiconducting nanowire.^[14] Here, we investigate the PEDOT:PSS/N-Si heterojunction by employing both s-SNOM and scanning Kelvin probe microscope (SKPM). In this article, mobile carrier (electron) density of the device cross-sections are mapped, indicating strong interface band bending. Furthermore, a slope edge of PEDOT:PSS on N-Si is characterized by SKPM and s-SNOM. A potential-decreasing region with a thickness of ≈ 25 nm is found in the PEDOT:PSS layer, which acts as an electrical potential barrier to block electrons injecting into PEDOT:PSS. According to the result of s-SNOM measurement, we observe a space charge region with a thickness ≈ 27 nm in PEDOT:PSS layer close to the interface. The finding of space charge region in the PEDOT:PSS layer near the interface allows us to interpret photo-induced charge separation and surface passivation of the PEDOT:PSS/N-Si hybrid contact.

Our near-field optical measurements are conducted using the MIR s-SNOM system (Neaspec GmbH, Germany), which is shown in **Figure 1a**. During operation, a CO₂ laser shines on the metal-coated atomic force microscope (AFM) tip which operates with a tapping amplitude of about 40 nm at a tapping frequency $\Omega = 270$ kHz. The backscattered light from the tip is collected by a parabolic mirror and interferes with a reference signal (from the same CO₂ laser) through a Michelson interferometer to extract both the amplitude and the phase information. The collected signal is demodulated at higher harmonics $n\Omega$ to suppress the background scattering from the tip shaft and the sample (in this manuscript, $n = 3$).

To analyze the properties of organic/Si heterojunction, photovoltaic devices based on PEDOT:PSS/N-Si hybrid contact are fabricated. Here, PEDOT:PSS is defined by the highly conductive PH1000 for all devices and the related characterizations. Unlike traditional crystalline Si solar cells, junctions of these hybrid devices are formed through a straightforward solution process rather than a high-temperature ion-diffusion procedure.^[15] The device structure is shown in **Figure S1**, Supporting Information. Based on the capacity–voltage (C–V) measurements shown in **Figure S1c**, Supporting Information, a built-in potential over 0.7 V is observed. Such a high potential barrier is efficient enough for charge separation. But, the origin of this high built-in potential needs to be further investigated. As a result, mapping the carrier distribution of the PEDOT:PSS/N-Si interface is essential to understand its working mechanism. As illustrated in **Figure 1b**, a cross-section of PEDOT:PSS/N-Si interface is successfully fabricated for characterization. The PEDOT:PSS thickness is around 1 μm determined by scanning electron microscopy (SEM) measurement of the heterojunction cross-section. This thickness of PEDOT:PSS is only specialized for s-SNOM and SKPM mapping characterization not for solar cell application. A thick PEDOT:PSS allows us to characterize the interface easily. The detail of fabrication process can be found in Experimental Section.

To investigate the interface properties, the cross-section of PEDOT:PSS/N-Si interface is characterized by the s-SNOM system. **Figure 2a** shows the front view of the interface cross-section, and the scanned area is indicated by dotted red rectangle. From both phase and amplitude images, we find distinguishable contrast between PEDOT:PSS and N-Si. As illustrated in **Figure 2b**, the signal of phase image mainly comes from imaginary part of complex dielectric value of material.^[14] Regarding the amplitude image in **Figure 2c**, the signal is mainly correlated with the real part of material complex dielectric value.^[14] Interestingly, we observe a low-signal amplitude region in the Si side close to the interface. Since the carrier concentration below 10^{19} cm^{-3}

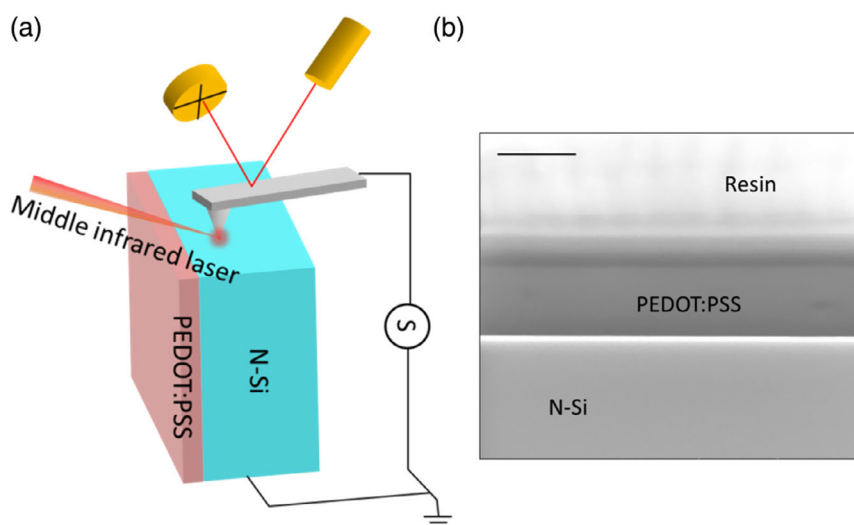


Figure 1. a) Schematic of infrared s-SNOM, where a horizontally polarized infrared CO₂ laser with wavelength (λ) of 11.086 μm is adopted as excitation source, which is focused onto a Pt/Ir-coated AFM tip by an off-axis parabolic mirror. b) SEM image of PEDOT:PSS/N-Si heterojunction cross-section, which is specially designed for interface mapping measurement. Scale bar is 1 μm .

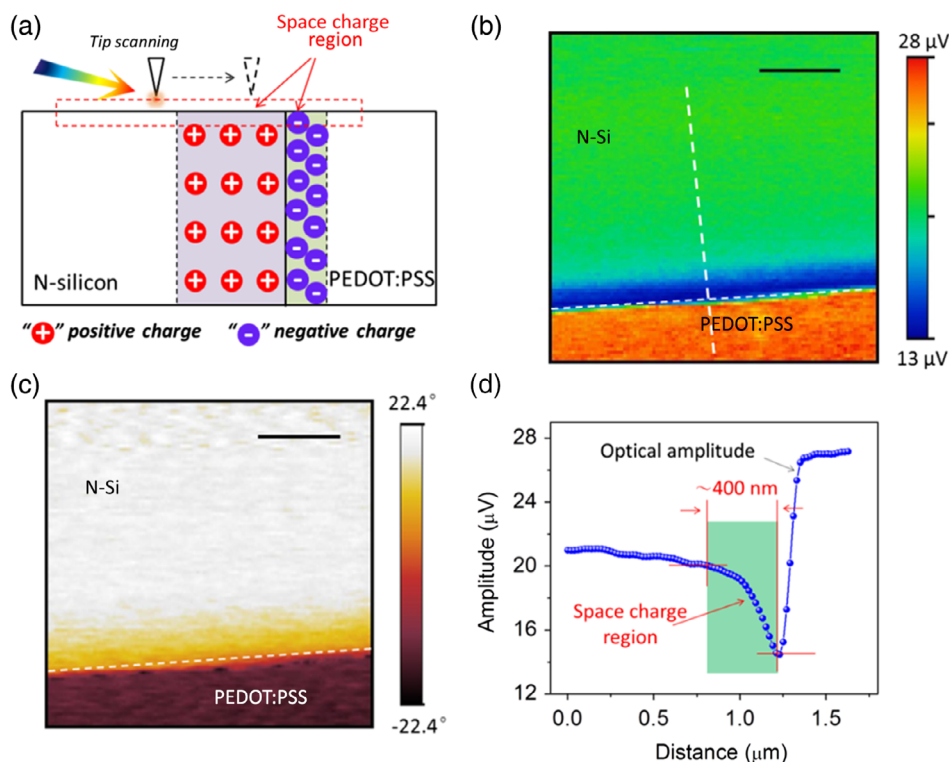


Figure 2. a) Scheme of interface cross-section mapping experiment (front view) using s-SNOM system (the scanned area is indicated by a dotted red rectangle). b) Optical amplitude and c) phase images of the device interface cross-section measured by s-SNOM system. Scale bar: 500 nm. d) Profile of cross-line from optical amplitude image.

in the Si is not sensitive to the 11.086 μm wavelength laser,^[16] the contrast in the Si side cannot be easily explained by the change of free carrier concentration. Depletion layer (space charge region), especially at the interface, usually takes place in semiconductors by applying electric field or contacting to a material with different work function. For example, in a traditional Si solar cell, there is a depletion layer at the junction area between p-type and N-Si. We believe the low-signal area in our Si sample (10^{17} cm^{-3} doping concentration) is ascribed to space-charge region because the dielectric value of space region is much lower than the neutral Si. According to the cross-line of amplitude image in Figure 2d, we find the space-charge region in Si is around 400 nm. This region is ascribed to electron transferring from Si to PEDOT:PSS because of the work function mismatch. As expected, it is very likely that a surface potential or carrier-density variation also occurs at PEDOT:PSS side due to charge transfer at the interface. Considering the limited space resolution ($\approx 20 \text{ nm}$), it is very challenging for us to observe carrier-density variation at PEDOT:PSS edge near Si side from the interface cross-section mapping measurements (see Figure 2c). An alternative experiment design is highly required to investigate carrier concentration in PEDOT:PSS.

A solution-processed PEDOT:PSS slope on N-Si is successfully built so that nanoscale mapping of the PEDOT:PSS side near the interface can be conducted. Figure 3c shows the 3D sketch of the SKPM measurement. The slope, with a fixed angle, can amplify the PEDOT:PSS thickness near the interface when mapping the lateral surface distance. Figure 3a plots the morphology of this

interface slope. According to the blue line shown in Figure 3d, the thickness gradually increases from edge to the center of the PEDOT:PSS slope. The boundary of this interface can be easily recognized through morphology cross-line where the height starts increasing. Surface potential simultaneously obtained at the same region reveals large potential difference between PEDOT:PSS and N-Si (as illustrated in Figure 3b). When comparing with the morphology cross-line at the same position, it is unsurprising to observe a potential drop in the Si side (left part of red line in Figure 3d), which is in line with the interface cross-section mapping characterization by s-SNOM in Figure 2. Being different from the device cross-section mapping, cross-line of surface potential on PEDOT:PSS slope exhibits a sharp drop at the interface (sky-blue rectangle part in Figure 3d). It means that, near the interface, surface potential difference exists in both Si and PEDOT:PSS, which helps sweeping generated charges out of the heterojunction. The potential drop region with a lateral surface distance around 1 μm has been observed. Considering the amplifying function of slope, we can infer from the sample morphology that the vertical thickness of potential drop region in PEDOT:PSS should be around 25 nm. This layer, existing potential drop near the interface, indicates a space charge region in PEDOT:PSS side, which shows electron blocking property to push electrons toward Si.

To confirm the existence of space charge region in PEDOT:PSS, s-SNOM system is adopted to map the carrier-density distribution of PEDOT:PSS slope. Figure 4c shows the front view of s-SNOM measurement, and the scanned area has been indicated

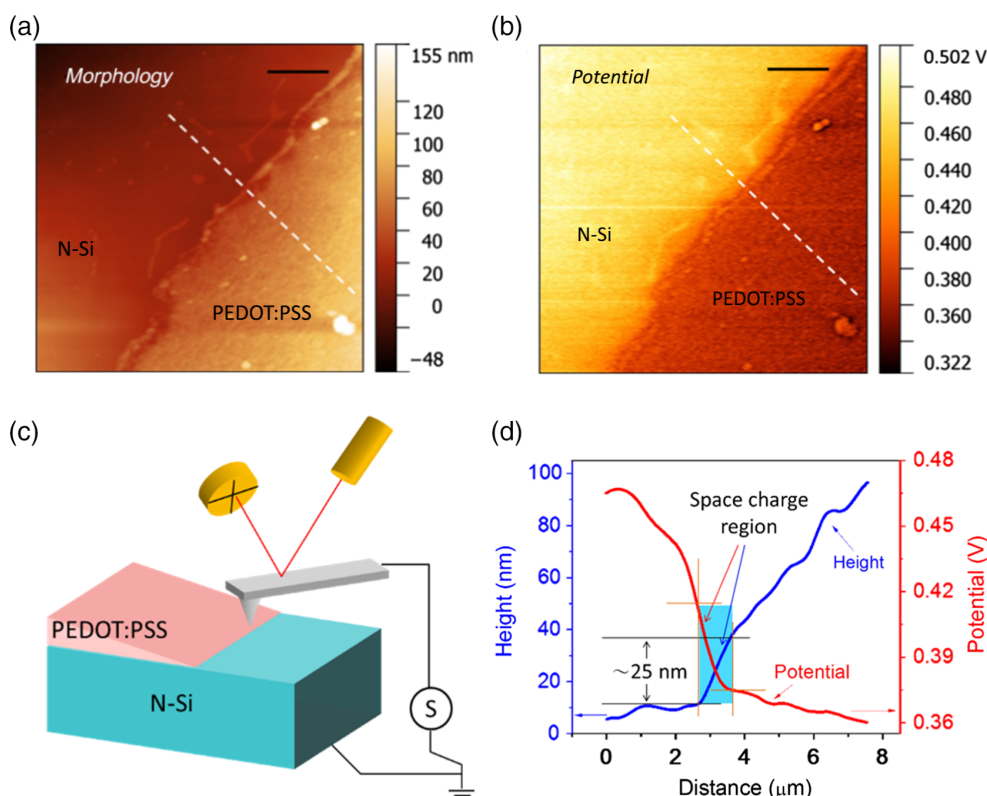


Figure 3. a) Morphology of PEDOT:PSS/N-Si interface with a PEDOT:PSS slope taken by SKPM system. Scale bar is 2 μm . b) Surface potential image of PEDOT:PSS/N-Si interface at the same region to the morphology. Scale bar: 2 μm . c) 3D view of slope scanning experiment using SKPM system. d) Cross lines of both height topography and surface potential extracted at the same place. The color region refers a potential drop zone in PEDOT:PSS layer near the interface.

in dotted red rectangle. The morphology and the simultaneous near-field optical amplitude images of scanned area are shown in Figure 4a,b. According to the contrast in optical amplitude image, we observed that the near-field optical signal of PEDOT:PSS slope near the interface is much lower than that of other PEDOT:PSS region. With the increasing PEDOT:PSS thickness, near-field optical amplitude gradually increases and finally saturates when PEDOT:PSS thickness is ≈ 65 nm (as illustrated in Figure 4d). Consequently, it can be deduced that the optical amplitude change along the slope originates from the charge-carrier variation in PEDOT:PSS itself rather than its morphology. The optical amplitude contrast along PEDOT:PSS slope is mainly caused by the carrier-density difference which exhibits resonance with infrared light. When contacting with N-Si, charge transfer takes place between PEDOT:PSS and N-Si. Thus, the free carrier density in PEDOT:PSS near the interface is much lower than that away from the interface, resulting in a space charge region in PEDOT:PSS side. However, considering efficient near-field interaction distance, probe depth of s-SNOM system should be taken into account when measuring the thickness of this space charge region.^[17] Hence, PEDOT:PSS slope on SiO_2 substrate acts as a reference. As shown in section ST1, Supporting Information, optical amplitude of PEDOT:PSS slope on SiO_2 also grows with increasing PEDOT:PSS thickness. It saturates when PEDOT:PSS thickness is over ≈ 38 nm. Since there

is no charge transfer between PEDOT:PSS and insulating SiO_2 , lower optical amplitude signal on PEDOT:PSS slope near the interface should come from SiO_2 substrate underneath. As a result, for PEDOT:PSS material, the probe depth of s-SNOM system is around 38 nm accordingly. Also, the real thickness of space charge region in PEDOT:PSS on N-Si substrate (≈ 65 nm) should subtract its probe depth (≈ 38 nm) of s-SNOM. A value of ≈ 27 nm ($65 \text{ nm} - 38 \text{ nm} = 27 \text{ nm}$) is obtained, which is in line with the thickness of potential drop region measured by SKPM (≈ 25 nm).

Typical current rectifying curves of PEDOT:PSS/N-Si heterojunction solar cell have been measured both in dark and under AM1.5 light illumination (Figure 5a). Surprisingly, without any optimizing of surface passivation, electrode contacts, and light harvesting, this heterojunction device yields power conversion efficiency (PCE) over 12% (the details can be found in Table S1, Supporting Information). According to the aforementioned discussion, we propose an energy-level alignment of PEDOT:PSS/N-Si heterojunction to interpret its efficient charge separation and surface passivation properties (as shown in Figure 5b). Due to the work-function difference, electrons in N-Si will move into PEDOT:PSS layer when contacting, generating a space charge region in Si. The electric field in space charge region in Si is so strong that an inversion layer at the interface has been induced (red rhombus in Figure 5b).

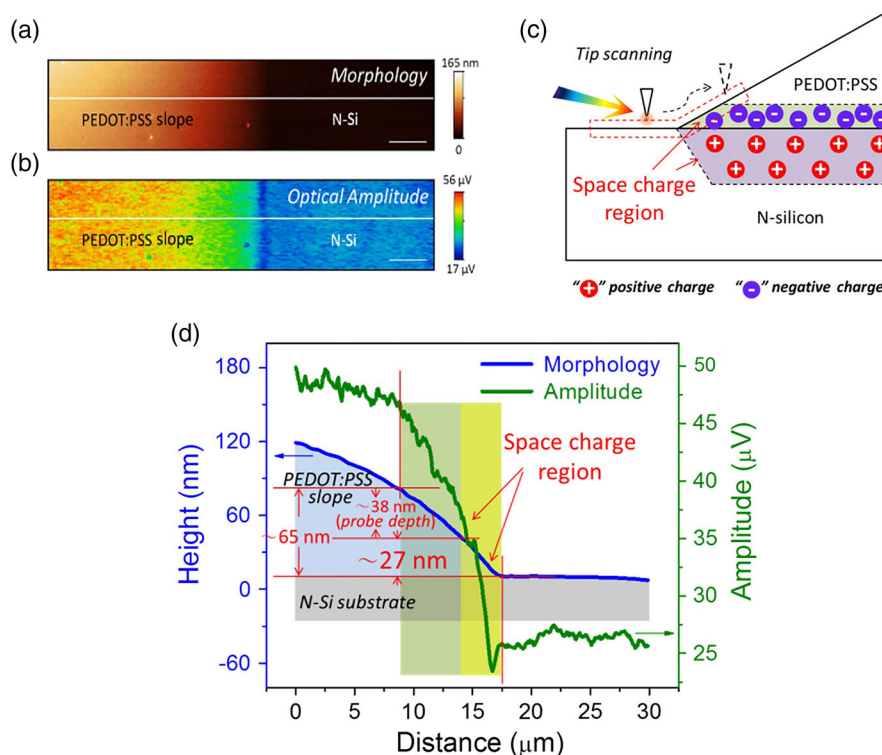


Figure 4. a) Morphology of PEDOT:PSS/N-Si interface with a PEDOT:PSS slope taken by s-SNOM system. Scale bar: 3 μm. b) Near-field optical amplitude image of PEDOT:PSS/N-Si interface at the same region to the morphology carried out at scanning laser with a wavelength of 11.086 μm. Scale bar is 3 μm. c) Scheme of slope scanning measurement (side view) using s-SNOM system. d) Cross-section lines of morphology and near-field optical amplitude extracted at the same place. The olive-color region refers space charge zone in PEDOT:PSS.

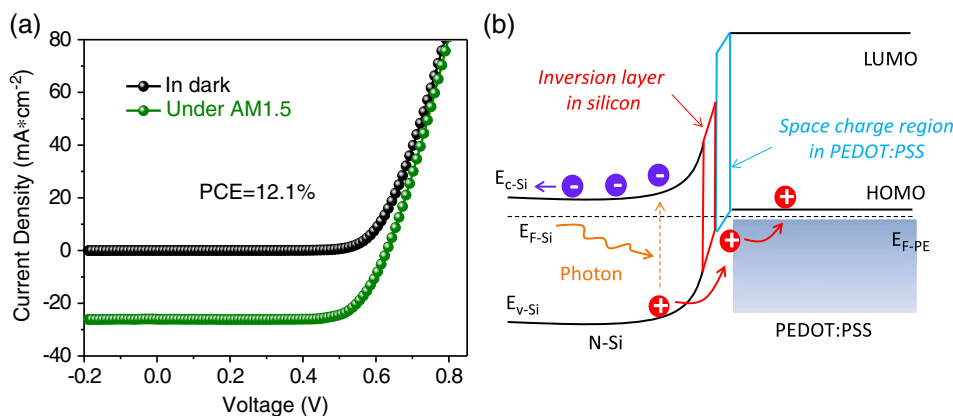


Figure 5. a) I-V curves of device in dark and under AM 1.5 light illumination. b) Schematic of the band structure of PEDOT:PSS/N-Si interface. Inversion layer in Si and low carrier-density region in PEDOT:PSS are included to interpret efficient charge separation of this heterojunction.

This layer forms a sharp barrier to block photo-induced electrons moving toward PEDOT:PSS. But due to the triangle-like barrier shape of the inversion layer in Si, electrons may still have chance to tunneling through the barrier, which would decrease the efficiency of photo-induced charge separation at the interface. In contrast, PEDOT:PSS can be described as a heavily doped p-type semiconductor. According to the Poisson's Equation, there should be a region in the PEDOT:PSS side with net inverse charges compared with the

silicon side, maintaining electric neutrality at the interface. Thus, the space charge region should also exist in the PEDOT:PSS layer near the interface (blue rhombus in Figure 5b), resulting in a large built-in potential (as shown in Figure S1c, Supporting Information). Thus, there should be an electron barrier in PEDOT:PSS to block photo-induced electrons transferring or tunneling through the interface. The space charge regions at the interface also reduce surface recombination rate of N-Si through field-effect passivation. As a result, minority

carrier lifetime of N–Si has drastically increased after spin-casting PEDOT:PSS (as shown in Figure S2, Supporting Information).

In summary, we have demonstrated that the novel charge-selective layer properties in PEDOT:PSS/N–Si heterojunction: space charge regions occur not only in N–Si but also in organic PEDOT:PSS. Electric field in space charge regions acts as main driving force for charge separation. Device interface cross-section characterization by s-SNOM and SKPM mapping indicates a space charge region in N–Si side near the interface. This region forms an electrical barrier to prevent photo-induced electrons from moving across the interface. For organic PEDOT:PSS side, a depletion region in PEDOT:PSS near the interface has been confirmed, which would form another electron barrier to decrease the chance of photo-induced electrons crossing the interface. Based on carrier mapping results, energy diagram with depletion regions in both side of PEDOT:PSS/N–Si heterojunction has been proposed. The depletion regions contribute to efficient charge separation property and also decrease surface recombination rate, which results in good surface passivation effect to N–Si. Our findings pave a way to enhance Si heterojunction solar cell performance via work function and conductivity modification of organic layer. This approach may enable us to characterize and optimize organic–inorganic heterojunction optoelectronic properties.

Experimental Section

Device Fabrication and Characterization: Highly conductive PEDOT:PSS (Heraeus PH 1000) solution, with the addition of 1 (wt%) Triton (Sigma-Aldrich) and 5 (wt%) dimethyl sulfoxide (DMSO), was used to fabricate a transparency conductive film on N–Si ((100)-oriented, 0.05–0.1 Ω cm resistivity) surface through spin-coating (3500 r min^{-1}) process. The solar cells were tested under AM 1.5G condition by a Newport 91160 solar simulator and a Keithley 2612 source meter. External quantum efficiency (EQE) of the device was characterized by Newport monochromator 74125. Also, capacitances versus voltage (C–V) measurements were conducted by a source meter (Keithley 4200-SCS) at frequency of 100 kHz.

Device Cross-Section and Interface Slope Preparation: The device cross-section was fabricated by a commercial ion milling system (Leica EM TIC 3X). First, the device edge was mechanically cleaved. Then, the freshly exposed cross-section was transferred into the vacuum chamber equipped with a liquid nitrogen cooling system. To get smooth cross-section, argon ions were used to mill the device edge with a beam voltage of 4 kV and current of 8 mA for about 3 h. After ion-milling process, samples are ready for further characterization. The interface slope is fabricated by drying a droplet of PEDOT:PSS solution on the clean N–Si surface.

Nanoscale Mapping Systems: Surface potential measurements were conducted by a commercial scanning probe microscope (SPM) system (Asylum Research, Oxford Instruments Company). Near-field optical experiments were conducted through a commercial s-SNOM system (NeaSNOM, NeaSpec GmbH).

Supporting Information

Supporting Information is available from the Wiley Online Library or from the author.

Acknowledgements

This work was supported by the National Natural Science Foundation of China (91833303, 61674108, 61604102, 61974099), the National Key

Research and Development Program of China (2016YFA0202402), Jiangsu High Educational Natural Science Foundation (18KJA430012), the Priority Academic Program Development of Jiangsu Higher Education Institutions, the 111 program and Collaborative Innovation Center of Suzhou Nano Science and Technology (NANO-CIC).

Conflict of Interest

The authors declare no conflict of interest.

Keywords

carrier redistribution, infrared scattering-type scanning near-field optical microscope, poly(3,4-ethylenedioxythiophene):poly(styrene sulfonate)/n-type silicon interface, scanning Kelvin probe microscopy

Received: July 12, 2019

Revised: September 7, 2019

Published online:

- [1] a) D. Adachi, J. L. Hernández, K. Yamamoto, *Appl. Phys. Lett.* **2015**, *107*, 233506; b) K. Yoshikawa, H. Kawasaki, W. Yoshida, T. Irie, K. Konishi, K. Nakano, T. Uto, D. Adachi, M. Kanematsu, H. Uzu, K. Yamamoto, *Nat. Energy* **2017**, *2*, 17032.
- [2] a) C.-H. Lin, S.-Y. Tsai, S.-P. Hsu, M.-H. Hsieh, *Sol. Energy Mater. Sol. Cells*, **2008**, *92*, 1011; b) E. Cabrera, S. Olibet, J. Glatz-Reichenbach, R. Kopecek, D. Reinke, Gunnar Schubert, *Energy Proc.* **2011**, *8*, 540; c) J. D. Fields, M. I. Ahmad, V. L. Pool, J. F. Yu, D. G. V. Campen, P. A. Parilla, M. F. Toney, *Nat. Commun.* **2016**, *7*, 11143.
- [3] M. J. Price, J. M. Foley, R. A. May, S. Maldonado, *Appl. Phys. Lett.* **2010**, *97*, 083503.
- [4] a) P. Yu, C. Tsai, J. Chang, C. Lai, P. Chen, Y. Lai, P. Tsai, M. Li, H. Pan, Y. Huang, C. Wu, Y. Chueh, S. Chen, C. Du, S. Horng, H. Meng, *ACS Nano* **2013**, *7*, 10780; b) F. Zhang, D. Liu, Y. Zhang, H. Wei, T. Song, B. Sun, *ACS Appl. Mater. Interfaces*, **2013**, *5*, 4678; c) J. Sheng, K. Fan, D. Wang, C. Han, J. Fang, P. Gao, J. Ye, *ACS Appl. Mater. Interfaces*, **2014**, *6*, 16027.
- [5] a) Y. Zhang, F. Zu, S. Lee, L. Liao, N. Zhao, B. Sun, *Adv. Energy Mater.* **2014**, *4*, 1300923; b) Y. Zhang, W. Cui, Y. Zhu, F. Zu, L. Liao, S. Lee, B. Sun, *Energy Environ. Sci.* **2015**, *8*, 297; c) J. He, M. A. Hossain, H. Lin, W. Wang, S. K. Karuturi, B. Hoex, J. Ye, P. Gao, J. Bullock, Y. Wan, *ACS Nano*, **2019**, *13*, 6356.
- [6] a) J. Chen, C. Con, M. Yu, B. Cui, K. W. Sun, *ACS Appl. Mater. Interfaces*, **2013**, *5*, 7552; b) P. R. Pudasaini, F. Ruiz-Zepeda, M. Sharma, D. Elam, A. Ponce, A. A. Ayon, *ACS Appl. Mater. Interfaces*, **2013**, *5*, 9620; c) M. Sharma, P. R. Pudasaini, F. Ruiz-Zepeda, D. Elam, A. A. Ayon, *ACS Appl. Mater. Interfaces*, **2014**, *6*, 4356.
- [7] a) M. Pietsch, M. Y. Bashouti, S. Christiansen, *J. Phys. Chem. C*, **2013**, *117*, 9049; b) J. P. Thomas, K. T. Leung, *Adv. Funct. Mater.* **2014**, *24*, 4978; c) J. P. Thomas, K. T. Leung, *Adv. Funct. Mater.* **2014**, *24*, 4978; d) J. He, Y. Wan, P. Gao, J. Tang, J. Ye, *Adv. Funct. Mater.* **2018**, *28*, 1802192.
- [8] a) S. Jeong, E. C. Garnett, S. Wang, Z. Yu, S. Fan, M. L. Brongersma, M. D. McGehee, Y. Cui, *Nano Lett.* **2012**, *12*, 2971; b) Y. Zhu, T. Song, F. Zhang, S. Lee, B. Sun, *Appl. Phys. Lett.* **2013**, *102*, 113504.
- [9] A. S. Erickson, A. Zohar, D. Cahen, *Adv. Energy Mater.* **2014**, *4*, 1301724.
- [10] S. Jäckle, M. Mattiza, M. Liebhaber, G. Brönstrup, M. Rommel, K. Lips, S. Christiansen, *Sci. Rep.* **2015**, *5*, 13008.

- [11] S. Jäckle, M. Liebhaber, C. Gersmann, M. Mews, K. Jäger, S. Christiansen, K. Lips, *Sci. Rep.* **2017**, 7, 2170.
- [12] E. T. Ritchie, D. J. Hill, T. M. Mastin, P. C. Deguzman, J. F. Cahoon, J. M. Atkin, *Nano Lett.* **2017**, 17, 6591.
- [13] A. C. Jones, R. L. Olmon, S. E. Skrabalak, B. J. Wiley, Y. N. Xia, M. B. Raschke, *Nano Lett.* **2009**, 9, 2553.
- [14] J. M. Stiegler, A. J. Huber, S. L. Diedenhofen, J. Gómez Rivas, R. E. Algra, E. P. A. M. Bakkers, R. Hillenbrand, *Nano Lett.* **2010**, 10, 1387.
- [15] C. Battaglia, A. Cuevas, S. De Wolf, *Energy Environ. Sci.* **2016**, 9, 1552.
- [16] a) A. J. Huber, D. Kazantsev, F. Keilmann, J. Wittborn, R. Hillenbrand, *Adv. Mater.* **2007**, 19, 2209; b) A. J. Huber, F. Keilmann, J. Wittborn, J. Aizpurua, R. Hillenbrand, *Nano Lett.* **2008**, 8, 3766; c) A. J. Huber, J. Wittborn, R. Hillenbrand, *Nanotechnology*, **2010**, 21, 235702; d) M. Wagner, A. S. McLeod, S. J. Maddox, Z. Fei, M. Liu, R. D. Averitt, M. M. Fogler, S. R. Bank, F. Keilmann, D. N. Basov, *Nano Lett.* **2014**, 14, 4529.
- [17] T. Taubner, F. Keilmann, R. Hillenbrand, *Opt. Express* **2005**, 13, 8893.